Journal of Materials Chemistry C

ROYAL SOCIETY OF CHEMISTRY

PAPER

View Article Online
View Journal | View Issue

Cite this: J. Mater. Chem. C, 2021, 9, 6225

Tailoring the nonlinear absorption of fluorescent dyes by substitution at a boron center†

Borys Ośmiałowski, *[a] Elizaveta F. Petrusevich,[b] Katarzyna C. Nawrot,[c] Bartłomiej K. Paszkiewicz,[d] Marcin Nyk,[c] Judyta Zielak,[a] Beata Jędrzejewska,[e] Josep M. Luis,[f] Denis Jacquemin *[g] and Robert Zaleśny *[b]

Received 5th January 2021,
Accepted 12th April 2021

DOI: 10.1039/d1tc00062d

rsc.li/materials-c

The tuning of the spectroscopic signatures of boron-carrying fluorescent dyes is achieved by subtle chemical modifications. In more detail, we propose a new series of compounds incorporating up to three electron-donating moieties around the central accepting core, using various positions for the donating moieties, including the central boron atom. For all dyes, a thorough experimental and computational investigation of the absorption and emission properties is presented, with specific emphasis on two-photon absorption. Our key finding is that the two-photon absorption cross section, a property vital for bioimaging applications, can be tuned to a large extent (eightfold increase) by changing the topology of the molecule and using an optimal substitution pattern, while mainly conserving the position of the absorption/emission band and fluorescence quantum yield. In addition, these dyes combine significant values of two-photon absorption cross sections (exceeding 500 GM) to significant fluorescence quantum yields – a beneficial feature for several applications.

1 Introduction

Emissive molecules have found applications in numerous fields including biolabeling,[1] molecular sensors,[2,3] and light emitting devices.[4] To this end, the optimization of the molecular structures is required to tailor the photophysical properties according to the needs of specific applications. Several fundamental properties of dyes can be relatively easily controlled: the position of both absorption and emission maxima, the molar attenuation coefficient (ε), and the affinity of dyes to other molecules. In contrast, some other features such as the fluorescence quantum yield (Φ) and the two-photon absorption (2PA) cross-sections ($\sigma^{(2)}$) are typically more difficult to predict based on chemical intuition. This is due to the complicated mechanisms related to the non-radiative processes for the former and to the inherent non-linear character of the latter. There are nevertheless some general methods to improve these two properties. For instance, one of the methods used for improving the fluorescence quantum yield is to increase the rigidity of the molecular skeleton. For instance, our group has demonstrated the attractiveness of this approach for a series of BF_2-carrying heterocycles by comparing phenantridines, quinolines, and isoquinolines.[5–7] The effect of the benzannulation manifested itself by a redshift of the emission band and a smaller Stokes shift while preserving the quantum yield.

In parallel to a high brightness ($\Phi \times \varepsilon$), the shift of absorption towards the red part of the spectrum is often needed for application of dyes in biolabeling. This is also a pivotal feature in the case of 2PA-based bioimaging, since the useful first biological window is located at *ca.* 650–1100 nm,[8,9] meaning that one-photon absorption should be in the 325–550 nm domain. The two easiest strategies to redshift both absorption and emission are to extend the π-conjugation path by introducing aromatic or ethynyl/ethenyl spacers, and by building push–pull structures. The former approach was shown to be successful for BODIPY dyes, for which the extensive tuning of π-conjugation by the addition of various aromatic groups impacts not only the

[a] Faculty of Chemistry, Nicolaus Copernicus University, Gagarina 7 PL-87100 Toruń, Poland. E-mail: Borys.Osmialowski@umk.pl
[b] Department of Physical and Quantum Chemistry, Faculty of Chemistry, Wrocław University of Technology, Wyb. Wyspiańskiego 27, PL-50370 Wrocław, Poland. E-mail: Robert.Zalesny@pwr.edu.pl
[c] Advanced Materials Engineering and Modelling Group, Faculty of Chemistry, Wrocław University of Science and Technology, Wyb. Wyspiańskiego 27 PL-50370 Wrocław, Poland
[d] Faculty of Microsystem Electronics and Photonics, Wrocław University of Science and Technology, Wyb. Wyspiańskiego 27, PL-50370 Wrocław, Poland
[e] Faculty of Chemical Technology and Engineering, UTP University of Science and Technology, Seminaryjna 3, PL-85326 Bydgoszcz, Poland
[f] Institute of Computational Chemistry and Catalysis and Department of Chemistry, University of Girona, Campus de Montilivi, 17003 Girona, Catalonia, Spain
[g] Université de Nantes, CNRS, CEISAM UMR 6230, F-44000 Nantes, France. E-mail: Denis.Jacquemin@univ-nantes.fr

† Electronic supplementary information (ESI) available: NMR spectra of compounds, data from the spectroscopic measurements, results from electronic-structure calculations. See DOI: 10.1039/d1tc00062d

absorption and emission maxima, but also the Φ values.[10] Indeed, this approach typically decreases the fluorescence quantum yield due to the increased flexibility that yields more efficient non-radiative pathways. The second approach to shift the optical spectra is to use groups of opposite accepting/donating character separated by a conjugated spacer, which means building a donor–acceptor architecture (DA-type molecules). This approach indeed allows creating an intramolecular charge-transfer (CT) transition.

It is indeed globally accepted that the presence of CT transition(s) is required to reach reasonably large values of 2PA cross section.[11] Compounds of various topologies have been designed following this strategy, and it is well recognised that the dipolar or quadrupolar character of the molecule has a great impact on its 2PA behavior. Notably, the 2PA responses of the DA-type BODIPYs have been studied several times[12–15] and their cross-sections were determined using fluorescencence properties,[12,13] which is reliable owing to BODIPY's large fluorescence quantum yield. However, for maximizing the 2PA, the application of π-extended symmetric DAD-like (donor–acceptor–donor) compounds has been very successful.[16–21] In the case of molecules with the DAD-type pattern, the angle between the lateral D and central A moieties does influence the 2PA response, highlighting that the relative orientation of the dipoles is a key factor.[16] To sum up, the number and relative arrangements of the donors and acceptors as well as the length of the conjugation path are important factors that can be changed in order to obtain desirable properties, but obtaining a good compromise remains a challenge.[22,23]

Although for fluoroborates the above described strategies for optimizing 2PA have been mainly applied by tuning the electron-donating groups and the π-conjugated segment, adding substituents to the boron atom, that acts as a Lewis acid, may be an alternative appealing approach. Indeed, the Lewis acidity of the boron atom can be controlled,[24,25] thus making the accepting properties of the B-carrying ring tunable. The Lewis acidity tuning may be achieved by directly adding suitable substituents to the boron (BR_2 as, for example, BF_2 *vs* $B(OMe)_2$) or by changing the R group in the $B(\text{-spacer-R})_2$ architecture.[26,27] For BODIPY dyes, such boron-functionalization is well-known and was achieved using a variety of methods, *e.g.*, (i) reaction of BF_2-group with $AlCl_3$ and methanol;[28] (ii) reaction of BF_2 with $AlCl_3$[29] (or BCl_3) and next *N*-nucleophiles[30] or *O*-nucleophiles;[31] and (iii) reaction with carbon-based nucleophiles.[32] All these modifications led to changes in the optical properties of the dyes. For instance, the BODIPY dye displayed on the left in Fig. 1 absorbs and emits at 526 and 550 nm, respectively, whereas for the mono-substituted (BFOR) and di-substituted ($B(OR)_2$) derivatives, the fluorescence maximum shifts to 546 and 540 nm, respectively.[31] In contrast, the absorption is unaffected by the changes between BFOR and $B(OR)_2$, allowing a fine control of the Stokes shift. Similar results have been obtained for BODIPYs substituted at boron with other nucleophiles.[30] In addition, we underline that introducing new chemical functions at the boron atom also allows controlling both solubility[33,34] and self-organization.[35,36]

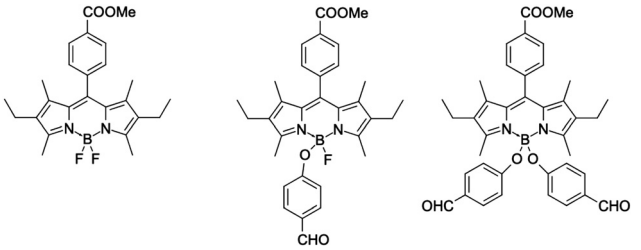

Fig. 1 BODIPY dyes substituted at boron atom.[31]

Putting together all these findings, it can be straightforwardly concluded that the DAD-type dyes with a boron center located in the middle of the conjugation path (see, for instance, the dyes displayed in Fig. 2) should develop properties that can be tuned by subtle changes in close proximity of (or at) the boron.[37,38] This approach may lead simultaneously to high fluorescence quantum yields, large Stokes shift, and sizeable values of the 2PA cross section. In addition, as illustrated in Fig. 2 one can go from the DAD pattern (MeO/NMe_2) to an AAD architecture by changing one group only (O_2N/NMe_2), which offers another hand to control the optical signatures. This variation of the electron density distribution was already successfully used in benzothiazoles bearing a BF_2 group,[38] as well as in regular BODIPYs.[39]

The fine tuning of the spectroscopic characteristics of the dye is the main motivation of the present study. We prepared and characterized new dyes showing modifications of the central part of a DAD-type system, allowing us to assess the impact of charge-transfer by tuning Lewis-acidity at the boron atom (Fig. 3). These molecules have been designed to obtain one, two, or three donor–acceptor sites in the same molecule. Additionally for comparison purposes, one parent molecule without electron-donating moieties and one dye of dipolar character have been synthesized as well. The modification at the boron atom leads to structures that present the substituent at the boron atom almost perpendicular to the π-conjugation plane. Recently, such axial substitution was used to develop lanthanum phtalocyanines exhibiting excellent non-linear properties.[40] A similar approach was used[41] in boron-carrying salicylic aldehyde derivatives and in boron subphtalocyanines.[42–45] We note that the orthogonality may be essential to control the 2PA parameters.[46] The aims of the current study are: (i) to characterise the absorption and emission properties of the six fluorophores exhibiting various charge-transfer strengths and orientations; (ii) to appraise the influence of distant substituents on the photophysical properties by modifying the Lewis acidity of the boron atom; (iii) to

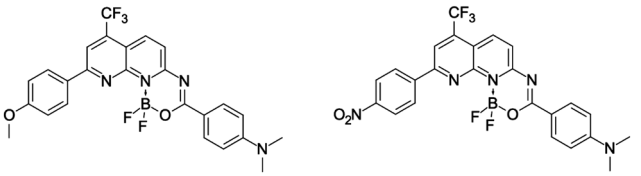

Fig. 2 The DAD- and AAD-type structures carrying the BF_2 group and exhibiting 2PA tuned by substituents.[37]

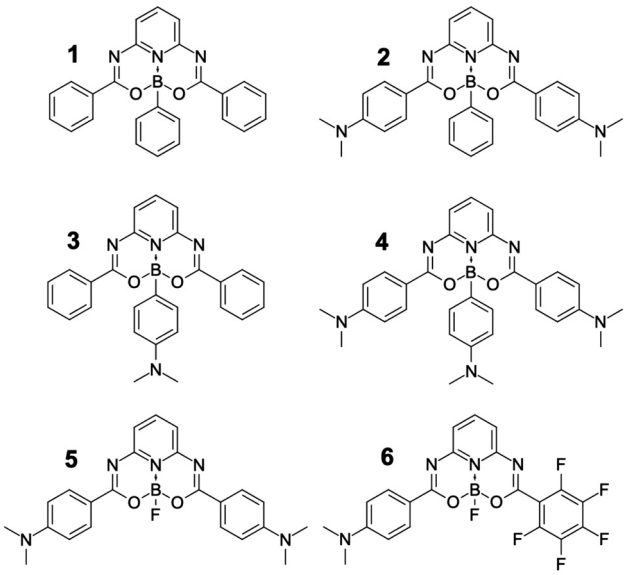

Fig. 3 The studied compounds **1–6**.

study the 2PA properties of these molecules and assess the usefulness of the modification of the boron electronic properties in fine-tuning the photophysical properties; and (iv) to investigate the influence of flexible NMe_2 group(s) placed at various positions on fluorescence quantum yield.

2 Results and discussion

Let us start this section by discussing the structural features of the six dyes. The equilibrium geometries of compounds **1–6** in chloroform solution optimized at the DFT level show, as expected, a perpendicular arrangement with the angles between the B-Ph phenyl plane and the plane formed by the oxygen atoms and pyridine nitrogen atom of 88.3°, 89.0°, 89.3° and 88.8° for **1**, **2**, **3**, and **4**, respectively. The crystal structures of compounds **1**, **3**, and **6** have been reported recently.[47] The same angle attains values of 88.7° and 87.9° in **1** and **3**, respectively. Considering the differences between the solid-state and the polar solvent environments, the DFT results are in very good agreement with the crystallographic data. To a large extent the B-Ph phenyl plane perpendicularity hampers the conjugation between the boron-attached substituent (Ph and $-C_6H_4-NMe_2$ groups) and the major π-conjugated plane of the molecule. Therefore, the changes in the dye properties are induced by tuning the Lewis-acidity of the boron atom only, and not by the direct conjugation effect between the moieties.

The experimental absorption spectra of all compounds recorded in $CHCl_3$ are shown in Fig. 4 ($\varepsilon(\lambda)$ [dm^3 mol^{-1} cm^{-1}] is shown in Fig. S1 in the ESI†). The first ($S_0 \rightarrow S_1$) band, demonstrating a clear vibrational fine structure for most compounds, has a maximum located in the visible region close to 450 nm for **2**, **4**, **5**, and **6** and at *ca.* 400 nm for **1** and **3** (Fig. 4), while the short wavelength band is at *ca.* 300 nm for **1** and **3** and 360–370 nm for the remaining derivatives. We underline that in **1** and **3** the blue-shifted band is *ca.* 40% more intense

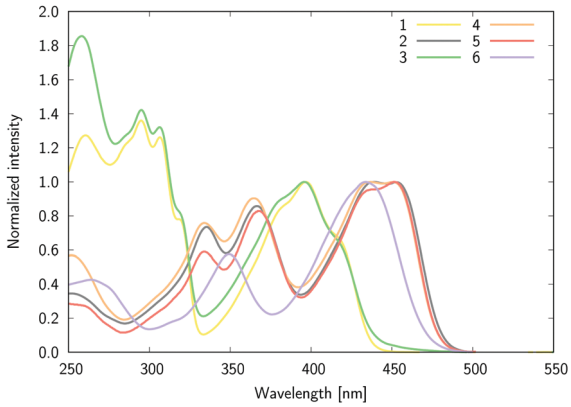

Fig. 4 The normalized absorption spectra of **1–6** in chloroform.

(higher ε) than its visible counterpart, whereas for the other four derivatives the second band has a slightly lower intensity than the first one.

The high similarity between the absorption spectra of **1** and **3** indicates that the boron functionalization does not influence the excitation from the ground to the excited states, as it only leads to a trifling bathochromic shift of the long-wavelength band for **1** *vs* **3** (2 nm). This outcome is found in all solvents (*vide infra*, Table 1), and is observed as well when comparing the spectra of **2** and **4**.

The mirror-shape of the emission as compared to absorption (Fig. 5) hints at small geometric reorganizations after excitation. Nevertheless, by comparing the respective bands in $CHCl_3$, one notices negligible variations between the absorption and emission spectra for **1**, **3** and **6**, but slightly different spectra for **2**, **4** and **5** (compounds carrying lateral NMe_2 groups). In the latter, the absorption spectrum clearly shows a vibronic structure in chloroform, with a separation of *ca.* 700 cm^{-1} between the peaks, while the fluorescence spectra display one sharp maximum with a shoulder red-shifted by 1010 cm^{-1}.

To obtain more insights into the character of the electronic states involved in absorption and emission, four solvents of various dielectric constants have been used for spectroscopic measurements (Table 1). Significant changes in the position of the $S_0 \rightarrow S_1$ absorption upon increase in polarity are observed for **2**, **4**, **5**, and **6**, whereas for both **1** and **3** almost no solvatochromism is noticeable, hinting at the lack of CT character in these two compounds, which is consistent with their molecular structure. In contrast, in **2**, **4** and **5**, positive solvatochromism is observed for both absorption and emission, indicative of a CT character. It is noteworthy that **3** could be considered as a CT dye as well due to the 1,4-substitution of the phenylene by a donor (NMe_2) and an acceptor (boron), but it was recently shown[47] that the putative 1,4-quinoid structure is absent in the phenylene in the ground state. Moreover, it was shown that the NMe_2 group in **6** donates more electron density than the same group in **3** allowing to the formation of the 1,4-quinoidal structure.[47] The attenuation coefficients (given in [dm^3 mol^{-1} cm^{-1}]) of the CT dyes **2**, **4**, **5**, and **6** are in the 32 000 and 48 300 range (except for methylcyclohexane), whereas for **1** and **3** we measured values in the

Table 1 The absorption maxima (λ_{abs}, [nm]), molar attenuation coefficients (ε, [dm^3 mol^{-1} cm^{-1}]), fluorescence maximum (λ_{flu} [nm]), Stokes shift (Δ_{SS}, [cm^{-1}]) and fluorescence quantum yields (Φ) of **1–6** in selected solvents (MCH – methylcyclohexane, chloroform, THF – tetrahydrofuran, ACN – acetonitrile)

	MCH	$CHCl_3$	THF	ACN
1/λ_{abs}	398	397	398	394
ε	17 400	18 600	20 200	20 600
λ_{flu}	**465**	**466**	**466**	**463**
Δ_{SS}	3620	3730	3666	3782
Φ	0.210	0.186	0.184	0.171
2/λ_{abs}	427.5	439	453	447
ε	—	46 200	43 600	48 700
λ_{flu}	**467**	**485**	**485**	**508**
Δ_{SS}	1979	2160	1456	2686
Φ	0.414	0.446	0.476	0.278
3/λ_{abs}	386.5	395	396	393
ε	16 600	16 300	21 800	17 000
λ_{flu}	**509**[a]	**467**	**467**	**463**
Δ_{SS}	6227	3903	3839	3847
Φ	0.045	0.015	0.006	0.004
4/λ_{abs}	425	437	433	446
ε	—	43 200	48 300	32 400
λ_{flu}	**463**	**489**	**481**	**499**
Δ_{SS}	1931	2433	2305	2281
Φ	0.432	0.106	0.018	0.011
5/λ_{abs}	422.5	452	450	449
ε	–	47 800	46 800	38 200
λ_{flu}	**459**	**484**	**482**	**510**
Δ_{SS}	1882	1463	1475	2644
Φ	0.439	0.385	0.511	0.089
6/λ_{abs}	430	434	430	429.5
ε	—	40 200	36 400	39 800
λ_{flu}	**459**	**525**	**480**	**480**
Δ_{SS}	1469	3994	2422	2450
Φ	0.319	0.041	0.002	0.001

[a] A similar redshift in fluorescence was observed in non-polar toluene with clearly visible two bands in fluorescence and larger intensity of the red-shifted band.

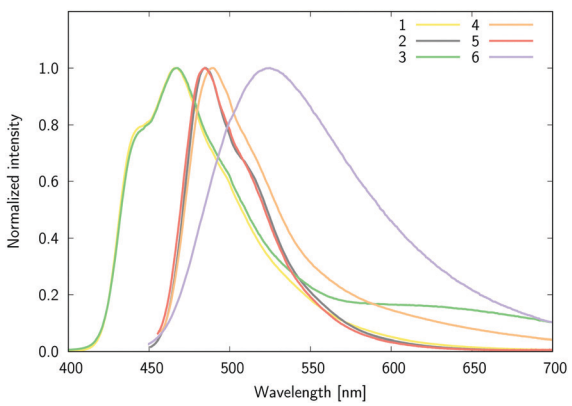

Fig. 5 The normalized fluorescence for **1–6** in chloroform. Except 1 and 3, the spectra were recorded in the 450–700 nm range.

16 600 to 21 800 range. With possible bioimaging applications in mind, additional measurements were also performed for selected dyes in DMSO/water mixtures. The results, presented in the ESI† (Fig. S2–S7), demonstrate solubility and stability of dyes in DMSO/water mixtures.

As stated above, a comparison of the data obtained for **1** and **3** indicates that the NMe_2 group attached to the phenylene ring does not significantly impact the spectral properties (see Table 1). However, a comparison of the fluorescence quantum yields measured in the **1–4** series, demonstrates that the Φ value is higher in **2** than in **1** (by 0.26) and larger in **4** than in **3** (by 0.091). Therefore, adding the NMe_2 group to the lateral parts of the conjugated DAD-type molecules improves the emission, likely because of the stiffening brought by contributions from the 1,4-quinoid-type structure. A similar effect was observed in other difluoroborates carrying conjugated electron-donating groups of similar efficacy.[48] In contrast, the **3** *vs* **1** and **4** *vs* **2** comparisons show that the addition of the same NMe_2 group on the aromatic ring attached to boron significantly decreases the fluorescence quantum yield ($\Delta\Phi = -0.17$ and $\Delta\Phi = -0.34$, respectively). This observation is, however, not fully preserved in methylcyclohexane, a non-polar solvent. Indeed, in this solvent, the fluorescence quantum yield for **4** slightly exceeds that of **2**. The two brightest molecules in all solvents are **2** and **5**. The introduction of phenyl instead of fluorine (**2** *vs.* **5**) seems to sterically protect the central part of the acceptor from interactions with surrounding solvent molecules yielding a three-fold increase in the fluorescence yield of **2** in acetonitrile. This steric hindrance may, on one hand, influence the efficiency of the non-radiative energy pathways originating from fluorophore–solvent interactions, and, on the other hand help in avoiding aggregation-induced quenching; both mechanisms contribute to larger Φ. The strength of the intermolecular interactions between a donor–acceptor-substituted dye in its electronic ground state and the environment usually increases with the polarity of the latter. This strength further increases in the excited states exhibiting an intramolecular charge transfer, as such dye typically undergoes an increase of its dipole moment after photon absorption. Therefore, the fluorescence quantum yield is usually reduced if the polarity of the solvent increases. Moreover, in very polar and protic environments, the protonation/deprotonation taking place between dye and solvent can also trigger non-radiative deactivation pathways.

Let us now discuss the electronic two-photon absorption spectra of compounds **1–6** (Table 2). Some of these structures might not exhibit significant two-photon absorption cross sections due to the lack of a clear push–pull nature; hence, we first performed the state-of-the-art electronic-structure calculations using coupled cluster theory to screen the properties prior to experimental measurements. Fig. 6 summarizes the CC2 results obtained for the three lowest-energy two-photon transitions. Note that these calculations

Table 2 Comparison of two-photon absorption cross-section of samples dissolved in chloroform using the Z-scan method

Compound	Wavelength [nm]	$\sigma^{(2)}$ [GM]	$\sigma^{(2)}/M$ [GM mol g^{-1}]
2	725	5.89×10^2	1.20
4	725	1.12×10^3	2.10
5	725	6.51×10^2	1.51
6	800	1.37×10^2	0.29

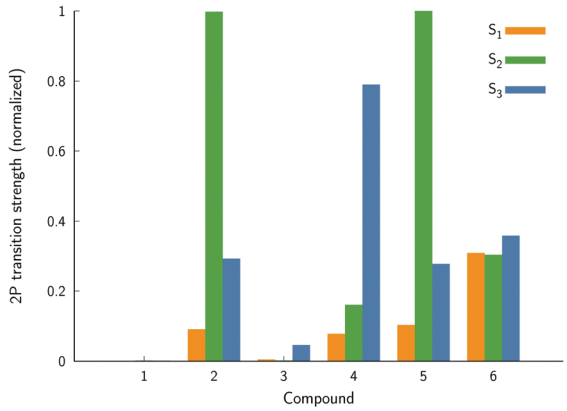

Fig. 6 The normalized two-photon transition strengths for molecules in chloroform calculated using the coupled-cluster CC2 method.

correspond to molecules in $CHCl_3$ solution. The key conclusion that can be drawn from the results shown in Fig. 6 is that compounds **1** and **3** show very low relative two-photon transition strengths, as compared to the other dyes. For this reason, we have not performed experimental measurements for these two compounds.

The experimental two-photon absorption spectra of compounds **2**, **4**, **5**, and **6** measured using the Z-scan technique in $CHCl_3$, are displayed in Fig. 7–10. These figures also contain wavelength-doubled one-photon absorption spectra for a direct comparison between one- and two-photon spectral features. In Fig. 7–10 we also show the results of CC2 calculations (indicated by points corresponding to one- and two-photon vertical excitations from the ground state to S_1, S_2, and S_3). The theoretical wavelengths were red-shifted by 50 nm (in one-photon spectra) to match the experimental features and allow easier comparisons. This deviation is typical of the selected level of theory, *e.g.* using very accurate reference as CAS-PT2/TZVP, one obtains a mean average error for a large set of organic molecules of 0.27 eV for CC2/TZVP.[49] The summary of electronic-structure calculations is shown in Table S1 in the ESI.†

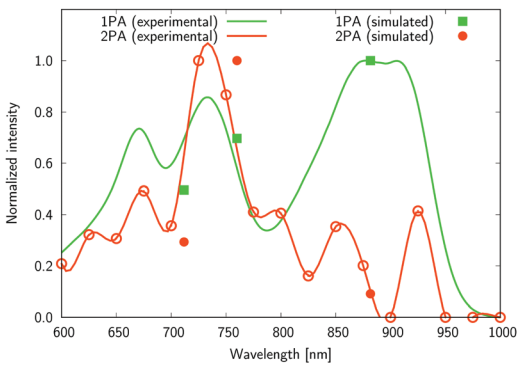

Fig. 7 The normalized one- and two-photon absorption spectra of **2** measured in chloroform. One-photon intensity is plotted against the wavelength multiplied by the factor of two. A red line connecting the experimental points (cubic spline) is used to guide the eyes. The theoretical values are given as closed symbols, whereas the open circles for the two-photon values correspond to experimental measures.

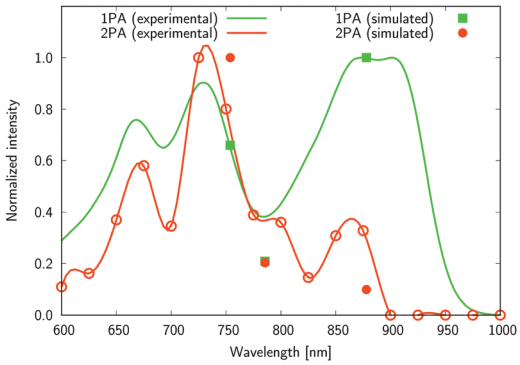

Fig. 8 The normalized one- and two-photon absorption spectra of **4**. See the caption of Fig. 7 for more details.

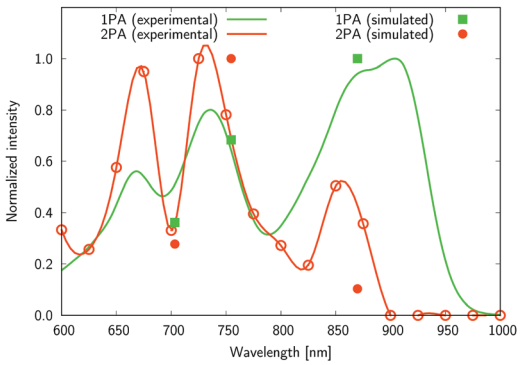

Fig. 9 The normalized one- and two-photon absorption spectra of **5**. See the caption of Fig. 7 for more details.

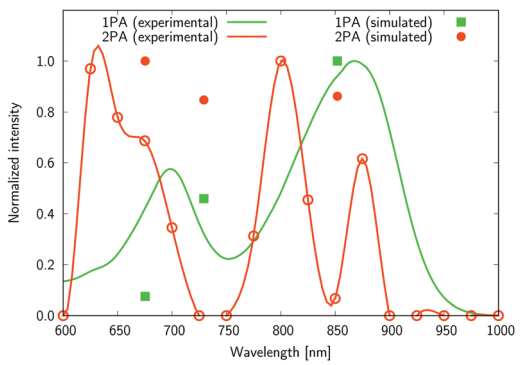

Fig. 10 The normalized one- and two-photon absorption spectra of **6**. See the caption of Fig. 7 for more details.

Several interesting conclusions can be drawn from the analysis of Fig. 7–10. First, the $S_0 \rightarrow S_1$ excitation does not yield the most intense two-photon response. The sole exception is compound **6** that present a 2PA spectrum showing two maxima of equal intensity. This specific results for **6** could have been crystal-balled. Indeed, relatively large values of two-photon absorption cross section for the $S_0 \rightarrow S_1$ transition are typically obtained in DA-type chromophores. Second, **2** exhibits very similar ratios of two-photon intensities at

725 and 850 nm similar to **5**. This highlights that replacing the fluorine atom bonded to the boron center by a $-C_6H_5$ moiety does not affect the nonlinear absorption spectra, at least in the 650–1100 nm range (first biological window). More quantitatively, the data listed in Table 1 demonstrate that the feature appearing at 725 nm in the experimental two-photon spectra of **2** and **5** corresponds to similar cross section values, *i.e.*, 589 GM (**2**) and 651 GM (**5**). Third, aiming at increasing the two-photon absorption cross section value, it is highly beneficial to introduce a strong electron-donating moiety onto the boron atom ($-C_6H_4-NMe_2$) – as shown by the results of Table 1, the $\sigma^{(2)}$ at 725 nm of **4** is roughly twice that of **2** or **5**. Fourth, we highlight that, by and large, the relative band intensities in one- and two-photon absorption spectra are very well reproduced by the electronic-structure calculations based on the CC2 method. This satisfactory performance of the CC2 method gives confidence that an in-depth analysis of two-photon activity in terms of electronic-structure parameters can be performed using this approach. To this end, we have employed the generalized few-state model (GFSM)[50] recently developed for electronic structure theories with a non-Hermitian structure.[51] GFSM allows interpreting the two-photon transition strengths in terms of electronic structure parameters:

$$\langle \delta_{0J}^{\mathrm{GFSM}} \rangle = \sum_K \sum_L \delta_{0JKL}^{\mathrm{GFSM}}, \text{ where}$$

$$\begin{aligned}
\delta_{0JKL}^{\mathrm{GFSM}} &= \frac{2}{15\Delta E_K \Delta E_L}(\alpha+\beta),\\
\alpha &= |\mu^{JK}||\mu^{K0}||\mu^{0L}||\mu^{LJ}|\\
&\quad\times\left(\cos\theta_{JK}^{K0}\cos\theta_{0L}^{LJ}+\cos\theta_{JK}^{0L}\cos\theta_{K0}^{LJ}+\cos\theta_{JK}^{LJ}\cos\theta_{K0}^{0L}\right)\\
\beta &= |\mu^{JL}||\mu^{L0}||\mu^{0K}||\mu^{KJ}|\\
&\quad\times\left(\cos\theta_{JL}^{L0}\cos\theta_{0K}^{KJ}+\cos\theta_{JL}^{0K}\cos\theta_{L0}^{KJ}+\cos\theta_{JL}^{KJ}\cos\theta_{L0}^{0K}\right)
\end{aligned} \quad (1)$$

In eqn (1), the superscripts distinguish between the right ($L0$) and left ($0L$) moments, $\Delta E_K = \frac{1}{2}\omega_J - \omega_K$, whereas the θ_{PQ}^{RS} terms represent the angle between the transition dipole moment vectors μ^{PQ} and μ^{RS}. Although the summations in eqn (1) for K and L run over all the electronic states, any number of intermediate states K and L can be chosen to obtain an approximate value. Here, we use both two- (2SM) and three-state models (3SM, intermediate state taken from the S_1–S_5 manifold), in which K and L can be either the ground state 0, the final excited state J (two-state model), or an intermediate state (three-state-model). Table 3 summarises the results of the GFSM analysis performed using the CC2 data for the most intense features in the electronic two-photon absorption spectra of compounds **2**, **4**, **5**, and **6**. The labeling "key state" denotes an intermediate state that recovers at least 50% of the two-photon transition strength computed using response theory. The results shown in Table 3 deliver a complementary piece of information to that obtained from the measurement. First, it is confirmed that compounds **2** and **5** exhibit similar electronic structure patterns as far as 2PA intensity is concerned. In particular, one finds that in both **2** and **5** the two-photon $S_0 \rightarrow S_2$ excitation is dominated, according to quantum-mechanical sum-over-state expression, by the product involving the $|\mu^{01}|^2 \cdot |\mu^{12}|^2$ transition moments. This indicates the importance of the intensity of the one-photon $S_0 \rightarrow S_1$ transition in the $S_0 \rightarrow S_2$ two-photon response. Hence, a possible route to further boost the two-photon $S_0 \rightarrow S_2$ intensity could be accomplished by chemical modifications enhancing the one-photon $S_0 \rightarrow S_1$ transition intensity. The same applies to two-photon $S_0 \rightarrow S_2$ intensity of dye **4**. However, there is a striking difference between compounds **2**/**5** and **4** in the case of two-photon $S_0 \rightarrow S_3$ excitation, namely, for the former pair of compounds, the three-state model is insufficient to describe the two-photon $S_0 \rightarrow S_3$ excitation, highlighting that contributions from high-lying excited states play a role, on the other hand, the two-photon $S_0 \rightarrow S_3$ intensity of **4** is dominated by the product involving transition moments $|\mu^{01}|^2 \cdot |\mu^{13}|^2$. In the case of the asymmetric dipolar structure **6** the two-photon $S_0 \rightarrow S_1$ intensity is, as expected, well described by the two-state model and the 0111 term makes the dominant contribution. This term involves the $S_0 \rightarrow S_1$ transition moment and the dipole moment of the S_1 excited state, typical of DA-type dyes. Nevertheless, the two-state model remains insufficient to describe the two-photon intensities to higher-lying states in that compound. Note that in the case of $S_0 \rightarrow S_2$ intensity of **6**, albeit the 0222 term is indicated as the largest one, the sum of symmetry related terms 0212 and 0221 prevails over the 0222 term.

Table 3 Summary of the key results obtained with the generalized few-state model calculations. See text for more details

Compound	Transition	2SM	3SM	Key state	Dominant $0JKL$ term
2	$S_0 \rightarrow S_2$	NO	YES	S_1	0211
	$S_0 \rightarrow S_3$	NO	NO		
4	$S_0 \rightarrow S_2$	NO	YES	S_1	0211
	$S_0 \rightarrow S_3$	NO	YES	S_1	0311
5	$S_0 \rightarrow S_2$	NO	YES	S_1	0211
	$S_0 \rightarrow S_3$	NO	NO		
6	$S_0 \rightarrow S_1$	YES			0111
	$S_0 \rightarrow S_2$	NO	YES	S_1	0222
	$S_0 \rightarrow S_3$	NO	YES	S_1	0311

3 Experimental

3.1 Synthesis and structure confirmation

The structure of compounds **1**, **3** and **5**–**6** has been already described,[47] while compounds **2** and **4** are new structures obtained in the same way as **1** and **3**. The only difference was the usage of the *N*,*N*-dimetylamino substituted substrate described in our previous publication.[52] 4-[(2*Z*,7*Z*)-7-[4-(Dimethylamino)phenyl]-5-phenyl-4,6-dioxa-2,8,13-triaza-5-borabicyclo[7.3.1]trideca-1(13),2,7,9,11-pentaen-3-yl]-*N*,*N*-dimethylaniline (**2**) orange solid, m.p. 246.5–248 °C. ^{1}H NMR (DMSO from TMS) δ: 8.06 (t, 1H), 8.04 (d, 4H, J = 9.1 Hz), 7.13 (m, 5H), 7.01 (d, 4H, J = 8.0 Hz), 6.77 (d, 4H, J = 9.1 Hz), 3.03 (s, 12H). ^{13}C δ: 165.33, 153.94, 150.53, 145.75, 131.19, 130.04, 128.09, 128.04, 118.80, 115.19, 111.52,

40.12. $C_{29}H_{28}BN_5O_2$ Calcd. C 71.17, H 5.77, N 14.31; found C 71.09, H 5.82, N 14.25. 4-[(2*Z*,7*Z*)-5,7-Bis[4-(dimethylamino)phenyl]-4,6-dioxa-2,8,13-triaza-5-borabicyclo[7.3.1]trideca-1(13),2,7,9,11-pentaen-3-yl]-*N*,*N*-dimethylaniline (**4**) orange-brown solid, m.p. 310 °C (dec.). ^{1}H NMR (DMSO from TMS) δ: 8.04 (d, 4H, J = 9.2 Hz), 8.02 (t, 1H), 6.97 (d, 2H, J = 8.0 Hz), 6.95 (d, 2H, J = 8.9 Hz), 6.67 (d, 4H, J = 9.2 Hz), 6.48 (d, 2H, J = 8.9 Hz), 3.03 (s, 12H), 2.73 (s, 6H). ^{13}C δ: 165.50, 153.87, 150.55, 131.15, 130.90, 119.13, 115.00, 112.37, 111.50, 40.13 (most quaternary carbons not visible in the spectra due to low solubility). $C_{31}H_{33}BN_6O_2$ caldc. C 69.93, H 6.25, N 15.78; found C 70.01, H 6.29, N 15.73. The NMR spectra are provided in the ESI† (Fig. S8–S11). The one-photon measurements were performed with the same equipment used in our previous works.[53]

3.2 Z-scan measurements

Chloroform solutions of **2**, and **4–6** were prepared (0.2%) for the Z-scan measurement, while **1** and **3** were excluded due to their lack of CT features and insignificant values of computed two-photon transition strengths. Spectrally-resolved nonlinear optical properties have been studied with the open aperture and the closed aperture Z-scan techniques using the following laser system: a Quantronix Integra-C Ti:sapphire regenerative amplifier producing ~130 fs, 800 nm pulses of 1 mJ energy per pulse with 1 kHz frequency and a Quantronix Palitra-FS optical parametric amplifier for wavelength tuning between 525 and 1100 nm. The Z-scan technique probes the changes in the signal from the laser beam as the sample is moved into and out of the region of the beam focus along the Z axis. The changes are monitored using three detectors: ''open aperture'' (OA) detector, ''closed aperture'' (CA) detector and reference detector. The first one measures the total power of the beam and thus indicates whether or not nonlinear absorption occurs. Only the central part of the beam is directed onto the CA detector; therefore, it allows to precisely detect changes in the geometry of the beam. The reference detector is set before the sample and the resulting signal is used to exclude any beam instabilities. To reduce data noise appearing in the traditional Z-scan technique we used a modified data acquisition system where the signal from the detectors is recorded by a data I/O acquisition card (*National Instruments* PCI-6143) with simultaneous sampling synchronized with the laser. Fig. S12–S15 in the ESI,† show representative open aperture and close aperture Z-scan measurement results at the maxima of nonlinear absorption, which were detected at 725 nm (**2**), 725 nm (**4**), 725 nm (**5**) and 800 nm (**6**), respectively, for the subsequent samples. In order to exclude the impact of molar mass on the results, we calculated a molar mass normalized merit factor $\sigma^{(2)}/M$ which, in fact, confirmed the ranking of the dyes as a function of their 2PA ability.

3.3 Computational methods

The ground state geometry optimization of structures **1–6** was performed at the CAM-B3LYP/cc-pVDZ level of theory[54,55] in a chloroform solvent modelled using the IEF-PCM method. The minima on the potential energy hypersurface were confirmed by evaluation of the Hessian at the same level. These calculations were performed using the GAUSSIAN 16 program.[56]

Molecular dynamics simulations were carried out for the rigid geometry of each dye in a cubic chloroform box of edge 50 Å using NAMD[57] combined with the CHARMM force field[58] and the chloroform force field of Dietz and Heinzinger.[59,60] The system was minimized for 10 000 steps followed by constant temperature NVT dynamics for 2 ns (1 step = 2 fs) at 300 K using a Langevin thermostat, periodic boundary conditions were applied. From the resulting trajectory, 50 snapshots were taken for further electronic-structure calculations.

Based on the results of the MD simulations, electronic-structure calculations were carried out using the resolution-of-identity coupled-cluster CC2 model[61] with the cc-pVDZ basis set[55] and the corresponding optimized auxiliary basis set.[62,63] In a study on 2PA of organoboron complexes it was showed that the differences between the two-photon transition strengths calculated at the RI-CC2/cc-pVDZ and RI-CC2/aug-cc-pVDZ levels do not exceed 5%.[51] The electrostatic embedding was used to account for the discrete solvent representation. These CC2 calculations were carried out with the TURBOMOLE V.7.3 program.[64] The results of electronic-structure calculations discussed in the body of manuscript were obtained for a single snapshot, selected to show the smallest deviation from the average $S_0 \rightarrow S_1$ excitation energy.

4 Conclusions

In this work, combining the results of experimental and theoretical investigations, we tuned the spectroscopic signatures of new fluorescent dyes by chemical substitution. To this end, starting with a A-shaped parent dye, a new series of derivatives have been designed to obtain one, two, or three donor–acceptor sites in the same molecule. The position of the NMe_2 group was found to be the key factor in the fine control of the position of the absorption and emission bands, the significant modification of the fluorescence quantum yield, and the strong variation of the amplitude of two-photon absorption cross-section. We underline that the two-photon absorption cross section can be boosted by substitution at the boron atom in the central moiety despite the insignificant conjugation of the substituent at this position. In other words, one can tune separately one- and two-photon optical signatures.

Importantly, these dyes, which have significant values of two-photon absorption cross sections (exceeding 500 GM for DAD-type dyes), preserve large fluorescence quantum yields in most of the solvents used. In contrast to the typical asymmetric DA-type architecture, the symmetrically substituted dyes exhibit the largest two-photon absorption cross sections for transitions to electronic excited states above S_1 (either S_2 or S_3), albeit still in the biological window. In short, this work clearly demonstrates that modifications at a boron center with appropriately chosen substituents can be an effective strategy for enhancing two-photon absorption properties while conserving the other properties so that they remain almost unaffected.

Conflicts of interest

There are no conflicts to declare.

Acknowledgements

R. Z., M. N., D. J., B. J. and B. O. acknowledge the financial support from the National Science Centre Poland (Grant No. 2017/26/M/ST5/00327). K. N. acknowledges the support from the National Science Centre Poland under Grant no. 2018/29/B/ST4/02172. J. M. L. is grateful for the financial support from the Spanish MICIN PGC2018-098212-B-C22 and the Catalan DIUE 2017SGR39. The Wroclaw and French teams are indebted to the CNRS for supporting their collaborations in the framework of the *ABSOLUTA* IEA project. The authors gratefully acknowledge Wroclaw Centre for Networking and Supercomputing as well as the CCIPL center installed in Nantes (France) for the generous allotment of computer time.

References

1 K. M. Dean and A. E. Palmer, *Nat. Chem. Biol.*, 2014, **10**, 512–523.
2 D. Wu, A. C. Sedgwick, T. Gunnlaugsson, E. U. Akkaya, J. Yoon and T. D. James, *Chem. Soc. Rev.*, 2017, **46**, 7105–7123.
3 B. Valeur and I. Leray, *Coord. Chem. Rev.*, 2000, **205**, 3–40.
4 L. Wang, L. Xiao, H. Gu and H. Sun, *Adv. Opt. Mater.*, 2019, **7**, 1801154.
5 A. Zakrzewska, R. Zaleśny, E. Kolehmainen, B. Ośmiałowski, B. Jędrzejewska, H. Ågren and M. Pietrzak, *Dyes Pigm.*, 2013, **99**, 957–965.
6 B. Ośmiałowski, A. Zakrzewska, B. Jędrzejewska, A. Grabarz, R. Zaleśny, W. Bartkowiak and E. Kolehmainen, *J. Org. Chem.*, 2015, **80**, 2072–2080.
7 A. M. Grabarz, B. Jędrzejewska, A. Zakrzewska, R. Zaleśny, A. D. Laurent, D. Jacquemin and B. Ośmiałowski, *J. Org. Chem.*, 2017, **82**, 1529–1537.
8 R. Weissleder, *Nat. Biotechnol.*, 2001, **19**, 316–317.
9 K. Podgorski, E. Terpetschnig, O. P. Klochko, O. M. Obukhova and K. Haas, *PLoS One*, 2012, **7**, 1–7.
10 S. Xu, R. E. Evans, T. Liu, G. Zhang, J. N. Demas, C. O. Trindle and C. L. Fraser, *Inorg. Chem.*, 2013, **52**, 3597–3610.
11 C. Katan, F. Terenziani, O. Mongin, M. H. V. Werts, L. Porrès, T. Pons, J. Mertz, S. Tretiak and M. Blanchard-Desce, *J. Phys. Chem. A*, 2005, **109**, 3024–3037.
12 J. Yang, Y. Rousselin, L. Bucher, N. Desbois, F. Bolze, H.-J. Xu and C. P. Gros, *ChemPlusChem*, 2018, **83**, 838–844.
13 L. Porrès, O. Mongin and M. Blanchard-Desce, *Tetrahedron Lett.*, 2006, **47**, 1913–1917.
14 D. Zhang, Y. Wang, Y. Xiao, S. Qian and X. Qian, *Tetrahedron*, 2009, **65**, 8099–8103.
15 X. Zhang, Y. Xiao, J. Qi, J. Qu, B. Kim, X. Yue and K. D. Belfield, *J. Org. Chem.*, 2013, **78**, 9153–9160.
16 K. Susumu, J. A. N. Fisher, J. Zheng, D. N. Beratan, A. G. Yodh and M. J. Therien, *J. Phys. Chem. A*, 2011, **115**, 5525–5539.
17 M. Albota, D. Beljonne, J.-L. Brédas, J. E. Ehrlich, J.-Y. Fu, A. A. Heikal, S. E. Hess, T. Kogej, M. D. Levin, S. R. Marder, D. McCord-Maughon, J. W. Perry, H. Röckel, M. Rumi, G. Subramaniam, W. W. Webb, X.-L. Wu and C. Xu, *Science*, 1998, **281**, 1653–1656.
18 S.-i. Kato, T. Matsumoto, T. Ishi-i, T. Thiemann, M. Shigeiwa, H. Gorohmaru, S. Maeda, Y. Yamashita and S. Mataka, *Chem. Commun.*, 2004, 2342–2343.
19 Y.-Z. Cui, Q. Fang, G. Xue, G.-B. Xu, L. Yin and W.-T. Yu, *Chem. Lett.*, 2005, **34**, 644–645.
20 S.-J. Chung, K.-S. Kim, T.-C. Lin, G. S. He, J. Swiatkiewicz and P. N. Prasad, *J. Phys. Chem. B*, 1999, **103**, 10741–10745.
21 D. Beljonne, W. Wenseleers, E. Zojer, Z. Shuai, H. Vogel, S. Pond, J. Perry, S. Marder and J.-L. Brédas, *Adv. Funct. Mater.*, 2002, **12**, 631–641.
22 A. Bhaskar, G. Ramakrishna, Z. Lu, R. Twieg, J. M. Hales, D. J. Hagan, E. Van Stryland and T. Goodson, *J. Am. Chem. Soc.*, 2006, **128**, 11840–11849.
23 B. Jędrzejewska, M. Gordel, J. Szeremeta, P. Krawczyk and M. Samoć, *J. Org. Chem.*, 2015, **80**, 9641–9651.
24 J. R. Lawson and R. L. Melen, *Organometallic Chemistry: Volume 41*, The Royal Society of Chemistry, 2017, vol. 41, pp. 1–27.
25 A. E. Ashley, T. J. Herrington, G. G. Wildgoose, H. Zaher, A. L. Thompson, N. H. Rees, T. Krämer and D. O'Hare, *J. Am. Chem. Soc.*, 2011, **133**, 14727–14740.
26 P. A. Deck, C. L. Beswick and T. J. Marks, *J. Am. Chem. Soc.*, 1998, **120**, 1772–1784.
27 I. B. Sivaev and V. I. Bregadze, *Coord. Chem. Rev.*, 2014, **270–271**, 75–88.
28 C. Tahtaoui, C. Thomas, F. Rohmer, P. Klotz, G. Duportail, Y. Mély, D. Bonnet and M. Hibert, *J. Org. Chem.*, 2007, **72**, 269–272.
29 C. A. Wijesinghe, M. E. El-Khouly, N. K. Subbaiyan, M. Supur, M. E. Zandler, K. Ohkubo, S. Fukuzumi and F. D'Souza, *Chem. – Eur. J.*, 2011, **17**, 3147–3156.
30 G. Zhang, M. Wang, F. R. Fronczek, K. M. Smith and M. G. H. Vicente, *Inorg. Chem.*, 2018, **57**, 14493–14496.
31 B. Brizet, C. Bernhard, Y. Volkova, Y. Rousselin, P. D. Harvey, C. Goze and F. Denat, *Org. Biomol. Chem.*, 2013, **11**, 7729–7737.
32 S. Goeb and R. Ziessel, *Tetrahedron Lett.*, 2008, **49**, 2569–2574.
33 G. Fan, L. Yang and Z. Chen, *Front. Chem. Sci. Eng.*, 2014, **8**, 405–417.
34 S. Zhu, J. Zhang, G. Vegesna, F.-T. Luo, S. A. Green and H. Liu, *Org. Lett.*, 2011, **13**, 438–441.
35 H. Manzano, I. Esnal, T. Marqués-Matesanz, J. Bañuelos, I. López-Arbeloa, M. J. Ortiz, L. Cerdán, A. Costela, I. Garca-Moreno and J. L. Chiara, *Adv. Funct. Mater.*, 2016, **26**, 2756–2769.
36 K. Yuan, X. Wang, S. K. Mellerup, I. Kozin and S. Wang, *J. Org. Chem.*, 2017, **82**, 13481–13487.
37 J. Dipold, E. E. Romero, J. Donnelly, T. P. Calheiro, H. G. Bonacorso, B. A. Iglesias, J. P. Siqueira, F. E. Hernandez, L. D. Boni and C. R. Mendonca, *Phys. Chem. Chem. Phys.*, 2019, **21**, 6662–6671.
38 M. A. Potopnyk, D. Volyniuk, M. Ceborska, P. Cmoch, I. Hladka, Y. Danyliv and J. V. Gražulevičius, *J. Org. Chem.*, 2018, **83**, 12129–12142.

39 P. K. Samanta, M. M. Alam, R. Misra and S. K. Pati, *Phys. Chem. Chem. Phys.*, 2019, **21**, 17343–17355.
40 B. Li, Z. Cui, Y. Han, J. Ding, Z. Jiang and Y. Zhang, *Dyes Pigm.*, 2020, **179**, 108407.
41 B. Zhang, S. Wang, J. Tan and X. Zhang, *Dyes Pigm.*, 2018, **155**, 186–193.
42 S. Shimizu, *Chem. Rev.*, 2016, **117**, 2730–2784.
43 Y. Takeuchi, A. Matsuda and N. Kobayashi, *J. Am. Chem. Soc.*, 2007, **129**, 8271–8281.
44 P. A. Stuzhin, I. A. Skvortsov, Y. A. Zhabanov, N. V. Somov, O. V. Razgonyaev, I. A. Nikitin and O. I. Koifman, *Dyes Pigm.*, 2019, **162**, 888–897.
45 S. Shimizu, T. Otaki, Y. Yamazaki and N. Kobayashi, *Chem. Commun.*, 2012, **48**, 4100.
46 M. M. Alam, M. Chattopadhyaya, S. Chakrabarti and K. Ruud, *Acc. Chem. Res.*, 2014, **47**, 1604–1612.
47 B. Dziuk, B. Ośmiałowski, B. Zarychta, K. Ejsmont and L. Chęcińska, *Crystals*, 2019, **9**, 662–678.
48 Y. Kubota, K. Kasatani, H. Takai, K. Funabiki and M. Matsui, *Dalton Trans.*, 2015, **44**, 3326–3341.
49 D. Jacquemin, V. Wathelet, E. A. Perpéte and C. Adamo, *J. Chem. Theory Comput.*, 2009, **5**, 2420–2435.
50 M. M. Alam, M. Chattopadhyaya and S. Chakrabarti, *Phys. Chem. Chem. Phys.*, 2012, **14**, 1156–1165.
51 M. T. P. Beerepoot, M. M. Alam, J. Bednarska, W. Bartkowiak, K. Ruud and R. Zalesny, *J. Chem. Theory Comput.*, 2018, **14**, 3677–3685.
52 A. M. Grabarz, A. D. Laurent, B. Jędrzejewska, A. Zakrzewska, D. Jacquemin and B. Ośmiałowski, *J. Org. Chem.*, 2016, **81**, 2280–2292.
53 B. Jędrzejewska, A. Skotnicka, A. D. Laurent, M. Pietrzak, D. Jacquemin and B. Ośmiałowski, *J. Org. Chem.*, 2018, **83**, 7779–7788.
54 T. Yanai, D. P. Tew and N. C. Handy, *Chem. Phys. Lett.*, 2004, **393**, 51–57.
55 T. H. Dunning, *J. Chem. Phys.*, 1989, **90**, 1007–1023.
56 M. J. Frisch, G. W. Trucks, H. B. Schlegel, G. E. Scuseria, M. A. Robb, J. R. Cheeseman, G. Scalmani, V. Barone, G. A. Petersson, H. Nakatsuji, X. Li, M. Caricato, A. V. Marenich, J. Bloino, B. G. Janesko, R. Gomperts, B. Mennucci, H. P. Hratchian, J. V. Ortiz, A. F. Izmaylov, J. L. Sonnenberg, D. Williams-Young, F. Ding, F. Lipparini, F. Egidi, J. Goings, B. Peng, A. Petrone, T. Henderson, D. Ranasinghe, V. G. Zakrzewski, J. Gao, N. Rega, G. Zheng, W. Liang, M. Hada, M. Ehara, K. Toyota, R. Fukuda, J. Hasegawa, M. Ishida, T. Nakajima, Y. Honda, O. Kitao, H. Nakai, T. Vreven, K. Throssell, J. A. Montgomery, Jr., J. E. Peralta, F. Ogliaro, M. J. Bearpark, J. J. Heyd, E. N. Brothers, K. N. Kudin, V. N. Staroverov, T. A. Keith, R. Kobayashi, J. Normand, K. Raghavachari, A. P. Rendell, J. C. Burant, S. S. Iyengar, J. Tomasi, M. Cossi, J. M. Millam, M. Klene, C. Adamo, R. Cammi, J. W. Ochterski, R. L. Martin, K. Morokuma, O. Farkas, J. B. Foresman and D. J. Fox, *Gaussian~16 Revision C.01*, Gaussian Inc., Wallingford CT, 2016.
57 J. C. Phillips, R. Braun, W. Wang, J. Gumbart, E. Tajkhorshid, E. Villa, C. Chipot, R. D. Skeel, L. Kalé and K. Schulten, *J. Comput. Chem.*, 2005, **26**, 1781–1802.
58 A. D. MacKerell, D. Bashford, M. Bellott, R. L. Dunbrack, J. D. Evanseck, M. J. Field, S. Fischer, J. Gao, H. Guo, S. Ha, D. Joseph-McCarthy, L. Kuchnir, K. Kuczera, F. T. K. Lau, C. Mattos, S. Michnick, T. Ngo, D. T. Nguyen, B. Prodhom, W. E. Reiher, B. Roux, M. Schlenkrich, J. C. Smith, R. Stote, J. Straub, M. Watanabe, J. Wiórkiewicz-Kuczera, D. Yin and M. Karplus, *J. Phys. Chem. B*, 1998, **102**, 3586–3616.
59 W. Dietz and K. Heinzinger, *Ber. Bunsen-Ges.*, 1985, **89**, 968–977.
60 W. Yu, X. He, K. Vanommeslaeghe and A. D. MacKerell Jr., *J. Comput. Chem.*, 2012, **33**, 2451–2468.
61 D. H. Friese, C. Hättig and K. Ruud, *Phys. Chem. Chem. Phys.*, 2012, **14**, 1175–1184.
62 F. Weigend, A. Köhn and C. Hättig, *J. Chem. Phys.*, 2002, **116**, 3175–3183.
63 C. Hättig, *Phys. Chem. Chem. Phys.*, 2005, **7**, 59–66.
64 *TURBOMOLE V7.3 2018, a development of University of Karlsruhe and Forschungszentrum Karlsruhe GmbH, 1989-2007*, TURBOMOLE GmbH, since 2007; available from http://www.turbomole.com.